



Research

Release of liquid CO₂ from the bottom of a duct



Osama M. Ibrahim¹  · André Vagner Gaathaug¹ · Per Morten Hansen¹ · Dag Bjerketvedt¹ · Knut Vaagsaether¹

Received: 11 April 2023 / Accepted: 12 August 2023

Published online: 25 August 2023

© The Author(s) 2023  OPEN

Abstract

This paper presents experimental results of the rapid phase transition of liquid CO₂ released from the bottom of a small rectangular duct (BR). The aim is to consider the factors influencing the phase transitions and the release rate if the rupture area is below the liquid level. The tests are initiated by rupturing the diaphragm separating the test section from an atmospheric chamber. Pressure and temperature measurements are used to analyze the phase transition. Also, a high-speed shadowgraph technique is used to visualize the waves. The results are compared with previous top-release tests (TR), where the rupture area is sited above the liquid level. Test results show that the duct's outlet flow behavior for the BR differs from the TR tests, wherein the gas/two-phase flow is choking. In the BR tests, the shadowgraph images demonstrate that when the liquid/two-phase flows out, the liquid/vapor interface remains nearly fixed until it breaks up. This behavior indicates that the headspace vapor has little influence on the initial evaporation in the BR tests. The results from the current BR tests indicate a lower degree of superheating than in the TR tests (it decreases by 34% for LVF = 66.0%), and the evaporation rate is 1.2–1.8 times faster.

✉ Osama M. Ibrahim, Osama.K.Ibrahim@usn.no; André Vagner Gaathaug, Andre.V.Gaathaug@usn.no; Per Morten Hansen, per.m.hansen@usn.no; Dag Bjerketvedt, Dag.Bjerketvedt@usn.no; Knut Vaagsaether, Knut.Vagsather@usn.no | ¹Faculty of Technology, Natural Sciences, and Maritime Sciences, Department of Process, Energy and Environmental Technology, The University of South-Eastern Norway, Kjølnes Ring 56, 3918 Porsgrunn, Norway.



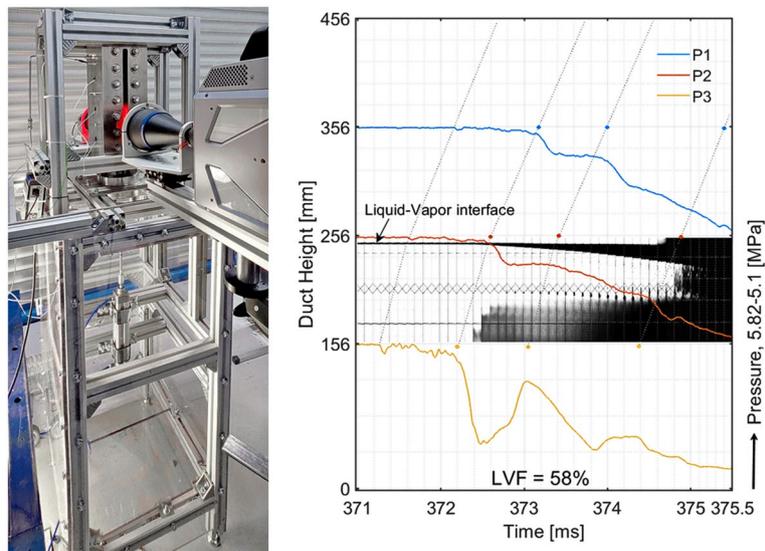
SN Applied Sciences

(2023) 5:247

| <https://doi.org/10.1007/s42452-023-05469-7>

SN Applied Sciences
A **SPRINGER NATURE** journal

Graphical abstract



Article Highlights

- The release below the liquid CO₂ level shows a distinct expansion wave structure.
- Faster evaporation during bottom-release tests than in top release.
- Shadowgraphs show the liquid/vapor interface's evolution during bottom-release tests.

Keywords Bottom release · Rarefaction wave · Evaporation wave · Phase transition · Two-phase flow

1 Introduction

Catastrophic failure of a pressurized CO₂ vessel may lead to boiling liquid expanding vapor explosion (BLEVE). Overfilling, overheating, flying fragments, fatigue, or corrosion may cause such events. The consequences include damaging blast waves, hazardous flying fragments, and the discharge of fluids into the surroundings [1]. It is crucial in designing and operating CO₂ infrastructure to understand the processes involved in the accidental release of liquified CO₂. This knowledge is required to predict, control, and prevent potential hazards.

An example of such a BLEVE event is the CO₂ accident in Repcelak, Hungary 1969. The accident was caused by overfilling a vessel containing 35 tons of CO₂ at 1.5 MPa, and – 30°. That vessel ruptured, creating a flying fragment that hit and burst another vessel under the liquid level. That vessel was pulled from its foundation and rocketed to a process laboratory distance away. Nine persons died due to the explosion's consequences [2].

When the vessel ruptures below the liquid level, the expansion wave propagates upwards through the liquid and vapor, as shown on the right side of Fig. 1. As a result, the liquid is directly pushed out into the surroundings. Due to the fast phase transition, a shock wave is generated in the air outside the vessel. Evaporation occurs at the same time inside and outside the vessel. The vaporization

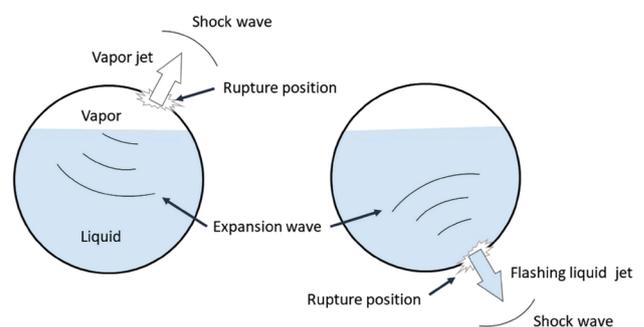


Fig. 1 Schematic drawing showing the release of pressurized liquified gas from a vessel during rupturing from the top (left) and the bottom (right)

process inside the vessel is mainly influenced by the vapor headspace expansion followed by its condensation. The expanded vapor condenses due to the expansion wave from the rupture vent and expansion wave reflection on the vessel's top. When the vessel ruptures, the outflowing liquid instantly evaporates [3]. The drawing in Fig. 1 shows the differences in the structure between top-side and bottom-side releases.

When a vessel ruptures above the liquid level, the vapor pressure in the vessel rapidly decreases. Simultaneously, a rarefaction wave propagates downwards through the vapor headspace and the liquid. As the vapor expands, its temperature decreases and may partly condense and freeze. Moreover, during the expansion wave propagation, the liquid temperature rises above its atmospheric pressure boiling point and becomes superheated. It remains temporarily in a metastable state before the phase transition occurs. The evaporation wavefront propagates as a thin zone of tiny bubbles. The required latent heat for vaporization is acquired from the superheated liquid [4]. Subsequently, an expanded two-phase mixture propagates downstream of the wavefront, and the remaining liquid's vapor pressure and temperature decrease. If the latent heat provided by the liquid's sensible heat cannot evaporate the whole liquid, the residual liquid portion is released as a flashing jet outside [5].

High-speed filming is well suited to studying the characteristics of the expansion waves during the release of superheated liquids. Hansen et al. [6] examined the phase transition during the depressurization of liquid CO₂ in a rectangular duct from the vessel's top. A series of Schlieren images demonstrated the early stages of rarefaction and evaporation wave propagation. Accordingly, the evaporation wave propagated downward at 30–40 m/s. The evaporation wavefront velocities at different container inclination positions have been experimentally studied by Dewangan and Das [7]. The tests were conducted in transparent tubes, length of 0.5 m, filled with water. The tube was sealed with a plastic diaphragm and submerged in a constantly heated liquid container with transparent walls. The results showed an intricate relationship between evaporation wavefront velocity and tube inclination angle. As the angle inclination increased in the 5–30°, the wavefront velocity increased due to the vapor phase's faster movement. An insignificant wavefront velocity change was observed in a range of 30–45°. However, inclination between 45 and 90° gradually increased the wavefront velocity. Other optical techniques were also utilized in several studies. The high-speed photographs that illustrated the evaporation wave structure and determined its velocity were utilized in studies such as Simões-Moreira [8], Reinke [2], and Hill [9].

So far, there has been little discussion about the phase transition mechanisms during the release below the liquid level in a container. Venart et al. [10] discussed the effect of the liquid content on the evolution of a vessel's explosion due to overheating. If the temperatures rise in a vessel filled to the medium level, the walls could rupture at the vapor headspace with an elastically propagating crack. As the crack stretches below the liquid level, the vessel containment rapidly fails, releasing the contents into the surroundings. Consequently, the contents' expansion follows an isentropic flash evaporation. The resulting blast effects were found to be more severe in the BLEVE events with higher filling levels. Tosse et al. [11] examined the evaporation wave and contact surface structure development in a vertical polycarbonate tube during liquid CO₂ decompression. The paper compared wave structures during two tube membrane bursting regimes: on the top (vapor side) and bottom (liquid side). When the tube membrane burst on top, an evaporation wave was observed to propagate into the liquid with a velocity of 20–30 m/s while the contact surface vapor/two-phase mixture propagated upward. However, when the membrane burst on the bottom, the interface vapor/two-phase mixture was accelerated downward as evaporation proceeded at the two-phase mixture/liquid surface. Also, the liquid evaporated on the bottom side, but the flowing outwards velocity was much greater than the evaporation wave propagation inside the tube.

Shang et al. [12] recently performed experiments with explosive evaporation in a cube vessel of 17 dm³ to evaluate the rupture position impact on the explosion intensity. In a series of tests, the vessel with pressurized water was ruptured above, below the liquid level, or at the vapor/liquid interface. Analyses of the pressure measurements demonstrated that the rupture disc location significantly influenced the expansion of the two-phase flow out and inside the vessel. A rupture in the gas phase promoted explosive evaporation of the liquid with substantial two-phase outflow. The two-phase outflow decreased in size when the rupture disc was located at the gas–liquid interface. However, the pressure considerably rebounded. When the rupture was below the liquid level, the liquid phase had not expanded enough; it had become insufficiently superheated to cause significant pressure rebound.

Few experimental studies have been carried out on liquid CO₂ depressurization by rupturing the container below the liquid level. Hence, the present study demonstrates novel physical aspects of phase transition during CO₂ release below the liquid level. This work focuses on the rarefaction and evaporation wave characteristics inside a rectangular duct with the outlet pointing downwards. The experimental results should clarify whether the release rate and the behavior of expansion waves during bottom

release differs from previously reported results from top-release tests [13]. The structure of the study takes the form of four sections. The first introductory section overviews the research's background and importance. It also outlines examples from the relevant literature, indicating the main questions and the knowledge gap. The following section describes the experimental setup and procedure. Section 3 presents the results and discusses their implications and contradictions to the comparable research outcomes. The last section summarizes the findings and analysis and identifies areas for further research.

2 Setup and experimental procedure

The test setup was assembled to perform lab-scale experiments for studying rapid phase transition during the release of liquefied CO₂ to atmospheric pressure. Figure 2 illustrates the main components of the experimental installation. The setup includes a rectangular duct fixed to the upper part of an aluminum structure. It is a high-pressure vessel made of stainless steel with a total volume of 191 cm³.

The duct has opposite-side borosilicate glass windows, facilitating optical access. The duct's orifice is opened to the atmospheric chamber at the bottom of the aluminum structure with dimensions 0.50 × 0.59 × 0.97 m³. The chamber space is covered from all sides with polycarbonate sheets. It has two vents on the top and bottom with

a total area of about 0.01 m². The test section is sealed with a multi-layer diaphragm consisting of eight circular aluminum foil pieces with a total thickness of about 0.8 mm. Two gaskets, primarily fabricated of glass, aramid fibers, and nitrile binder, were attached to both sides of the diaphragm to prevent possible leaks. The diaphragm with affixed gaskets is firmly pressed at the duct's opening between two flanges with four bolts. Figure 3 shows the rectangular duct's dimensions in (a) and an image of the experimental installation in (b).

The gaseous and the liquid CO₂ are supplied to the duct from industrial-grade cylinders equipped with control valves, a dip tube for liquid, and a regulator for gaseous. The diaphragm is punctured with an arrow-shaped needle fastened to a rod pneumatic cylinder actuator which is accurately aligned with the duct's orifice. The pressure in the duct is recorded using three Kulite XTM-190-2000G piezoresistive transducers mounted alongside the duct sidewall. The distance between a transducer and the adjacent one is 100 mm. These transducers have a measuring range of 0–140 bar, a natural frequency of 410 kHz, and a measurement accuracy of ± 1.4 bar.

Furthermore, the duct is instrumented on the top and bottom with two K-type thermocouples with an accuracy of ± 1%. The moving average filter was used to smooth the recorded data. The data acquisition system (DAQ) includes three HBM Quantum modules, two MX410, and one MX440B. Their recorded data at 96 kHz are transferred to a computer through a hub.

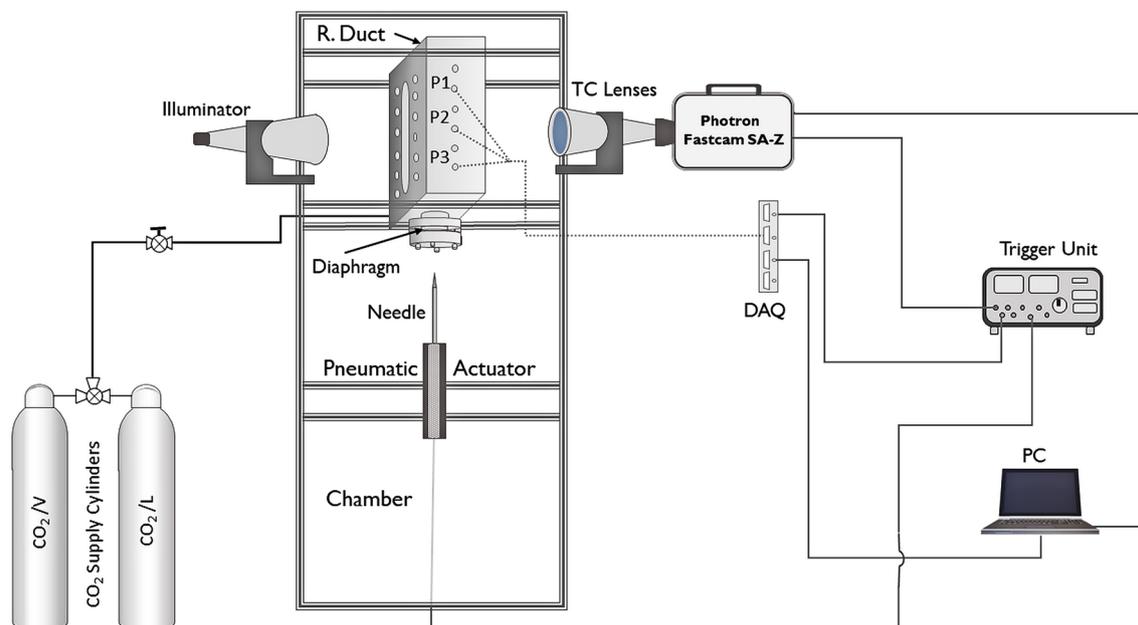


Fig. 2 Schematic drawing of setup for CO₂ depressurization in a rectangular duct with the opening pointing downwards. DAQ Data Acquisition system, TC Telecentric

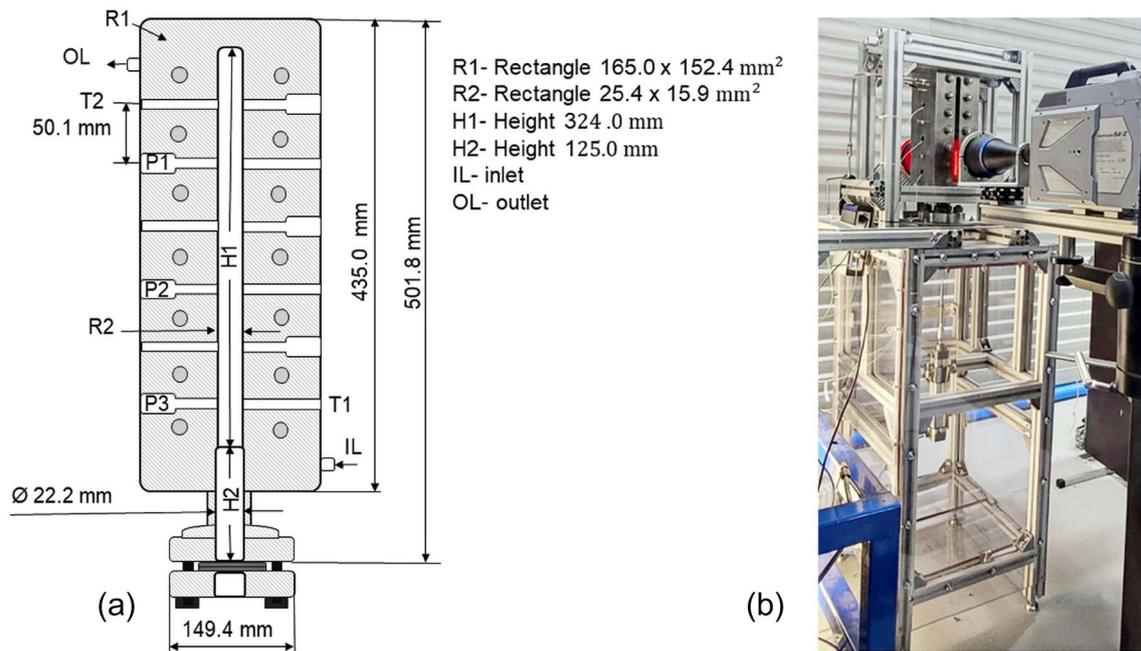


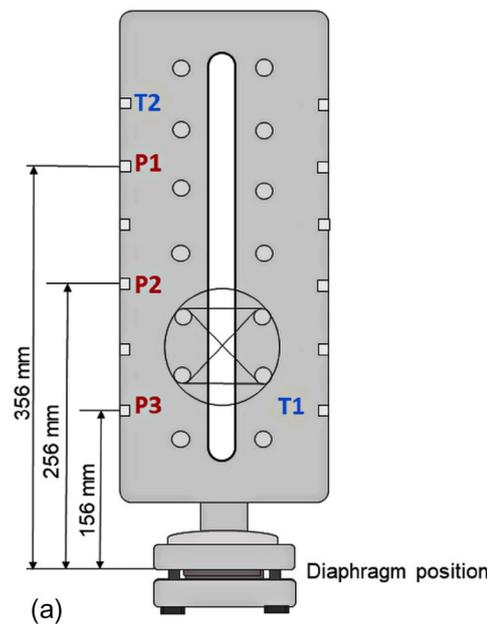
Fig. 3 **a** The high-pressure duct's dimensions. **b** Photograph of the experimental arrangements

The phase transition process during depressurization inside the duct is visualized by shadowgraph imaging. This technique visualizes the density gradients. A different lighting pattern is produced due to the refractive deflection of a light ray forming a light area on the captured plane. Shadowgraph configuration involves

Telecentric TC lenses manufactured by OPTO ENGINEERING and high-performance illuminator LTCLHP.

The illuminator was installed perpendicular to the windows, and its beam covers about 90 mm of the duct's height between pressure transducers P2 and P3. Also, the images were captured by a high-speed camera Photron

Fig. 4 **a** Sketch of the test section showing the pressure transducer positions and the distance from the diaphragm position **b** photograph of the duct showing the positions of the shadowgraph lenses and pressure transducers



SA-Z at 50,000 fps and a resolution of 256×1024 pixels. Figure 4 (a) shows a sketch defining the sensor positions, while (b) is a photograph illustrating the location of the shadowgraph lenses and pressure transducers in (b).

The duct was flushed with CO_2 vapor at 1 MPa before every experiment, then filled with liquid CO_2 to the required level. It remained for about 10 min to stabilize before the test started. The temperature gave the equilibrium state at a particular time. The Quantum pulse generator initiated the depressurization tests by synchronously triggering the pneumatic actuator, the DAQ system, and the high-speed cameras. Due to the actuator's piston movement, the needle punctured the diaphragm entirely with a time delay of about 400 ms. MATLAB and Photron FASTCAM Viewer Software were used to analyze pressure and temperature recordings and high-speed images. The results were compared with previous results when the diaphragm was on top.

3 Results and discussions

A series of tests were performed to release pressurized CO_2 from the rectangular duct's bottom into the atmosphere. The experiments started by rupturing the diaphragm. The initial conditions were liquid/vapor at saturated pressure varying between 5.7 and 6.1 MPa, corresponding to the saturated pressure at ambient temperature. The duct was filled with CO_2 at different liquid volume fractions (LVF) 0, 29, 35, 41, 53, 58, 66, 77, 89, and 97% of the total volume.

3.1 Waves characterization

Figure 5 shows the pressure records for the first 35 ms after rupturing the diaphragm. Time 0 is the time of the

diaphragm rupture and the depressurization onset. Sensors (P1–P3) are positioned from top to bottom, as shown in Fig. 4. The LVF in Fig. 5 (a) was 29, (b) 53, (c) 66, and (d) 97% of the total volume. As seen in Fig. 5, all LVFs have a first decline in pressure caused by an expansion wave from the diaphragm rupturing. After the first expansion, the liquid is metastable. The metastable state duration depends on the LVF. This duration increased as the LVF increased, as shown in graphs (a–d), Fig. 5. Low LVF shows a gradual pressure decrease during the metastable state, while the highest LVF shows a near-constant pressure plateau.

The pressure records show a decrease after the metastable state, corresponding to the liquid's evaporation. In the last part of the experiments, the observed pressure decrease was due to the two-phase mixture outflow. Because of the limited liquid mass flow at the outlet, the liquid inside the duct required more time to evaporate. Also, for the LVF of 53% and higher, this trend can be seen as an increase in pressure. The evaporation-driven pressure increase is further profound for the higher LVFs. However, as the degree of superheating is expected to be small, the evaporation process could also occur due to heterogeneous nucleation at the duct's wall.

The velocities of the head of the rarefaction wave were calculated based on the records from the three pressure sensors. The graphical approach used to determine the velocities is described in an earlier study [14]. The calculated rarefaction wave velocities were 200 m/s for zones P2–P3 and P2–P1 in (a), with a LVF of 29%. For the LVF of 97% in (d), 299 m/s for zone P2–P3 and 285 m/s for P2–P1. The velocity calculation errors were estimated as ± 8 m/s. Furthermore, the speed of sound based on the Span-Wagner Equation of State's tabulated data [15] is calculated to be 311 m/s for the liquid phase and 193 m/s for the vapor at 5.87 MPa and 22.3 °C.

Fig. 5 Pressure transducer records during 40 ms release of liquid CO_2 from the bottom of a rectangular duct for LVFs of 29, 53, 66, and 97% in **a–d**, respectively

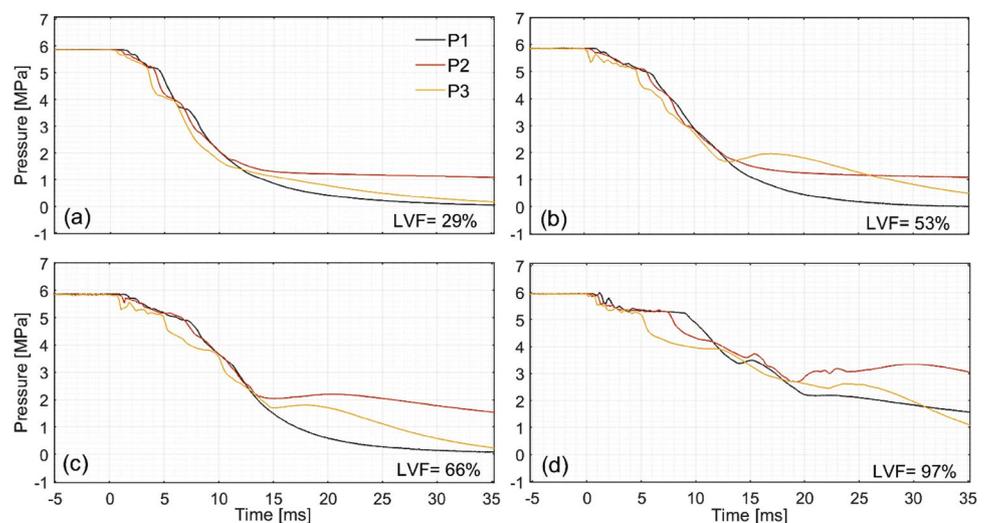


Fig. 6 Temperature sensors' records T1 (bottom) and T2 (Top) during 400 ms of CO₂ depressurization for LVFs of 29, 53, 66 and 97% in the graphs a–d, correspondingly

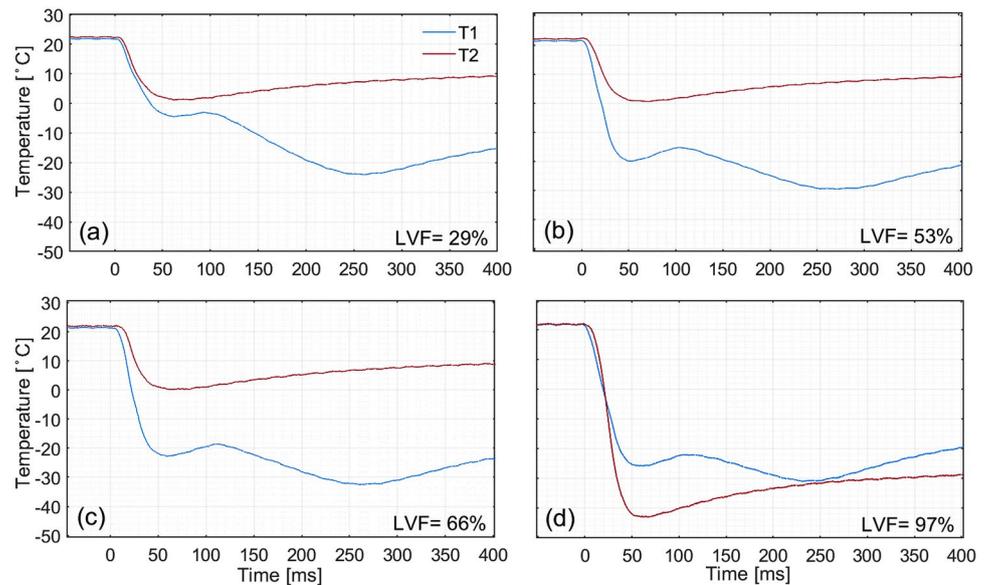


Figure 6 shows the temperature records for the first 400 ms after the diaphragm ruptured. The LVFs in the temperature graphs correspond to those in the pressure graphs in Fig. 5. Graphs in Fig. 6 from (a–c) show a slight reduction in the temperature (T1) as the evaporated liquid volume increased, while the temperature (T2) drop was nearly the same, around 0 °C.

Interestingly, the drop in temperature (T2) in Fig. 6d was more significant than the temperature decline during 50 ms depressurization. As the liquid level was above the two sensors, the liquid expansion and evaporation may have been essential factors in this temperature reduction. Comparing the temperature records with the pressure sensors measurements, for LVF of 97%, the atmospheric pressure was reached approximately after 50 ms (not shown in Fig. 5) while the temperature T2 does not reach the triple point (− 56.4 °C), it declined to − 42.4 °C and then started to recover. This indicates no dry ice formation, and the system is still in a non-equilibrium state. It may also be due to the relatively slow response of the temperature sensors.

3.2 Comparison of top and bottom duct releases

The results from the bottom release (BR) experiments were compared to those achieved previously by Hansen [13] from top release (TR) tests in the same duct. The aim is to describe the differences in the dynamic flow characteristics between the bottom (BR) and top (TR) releases of liquified CO₂. Figure 7 compares the pressure records inside the rectangular duct for TR (a and b) and BR (d and e) experiments. Enlarged segments of 3 ms from (b) and (e) are shown in Fig. 7c and f. P2 and P3 were below the liquid level in TR and BR tests.

The pressure decline during CO₂ decompression was faster in BR tests than in TR. As seen in Fig. 7b, it required about 17 and 26 ms for P2 and P3 to reach 2 MPa, while it required about 13.7 ms for BR in Fig. 7e. The most likely cause is that the downstream two-phase mixture was choking at the duct opening during the TR tests. (It can be seen in Fig. 7b that the fluctuations in the pressure lines have vanished after 2 MPa. After that, the pressure lines smoothly decline to atmospheric pressure. Then, the value of 2 MPa is specified for the comparison). The pressure decrease during BR tests resulted from the diaphragm rupturing and then the liquid mass outflow from the bottom. In TR tests, the liquid mostly evaporated inside the duct. However, evaporation occurred inside and outside the duct, and evaporation was faster during BR tests.

Furthermore, Simões-Moreira [8] defined the degree of superheating (DOS) as the maximum expansion in the metastable region. It is described by pressure drop from pre-ruptured pressure to the pressure of the superheated liquid in the metastable state. The first sharp decrease in liquid pressure (P2 and P3) in Fig. 7c and f is about 0.56 MPa for BR and 0.9 MPa for the TR. In addition, the DOS for LVF of 35% during BR is about 0.36, while it is 0.8 for LVF of 37% during TR tests (not shown in figures). The fact that a portion of the expanded liquid flowed out during BR could explain the small degree of superheating (DOS) attained compared to the TR experiment. The above observations about the faster evaporation and lower DOS during the BR tests compared to TR tests were supported by the conclusions made by Venart et al. [10], Tosse et al. [11], and Shang et al. [12]. These authors' results concerning rapid phase transition without choking conditions and more intense blast wave during BR experiments indicate

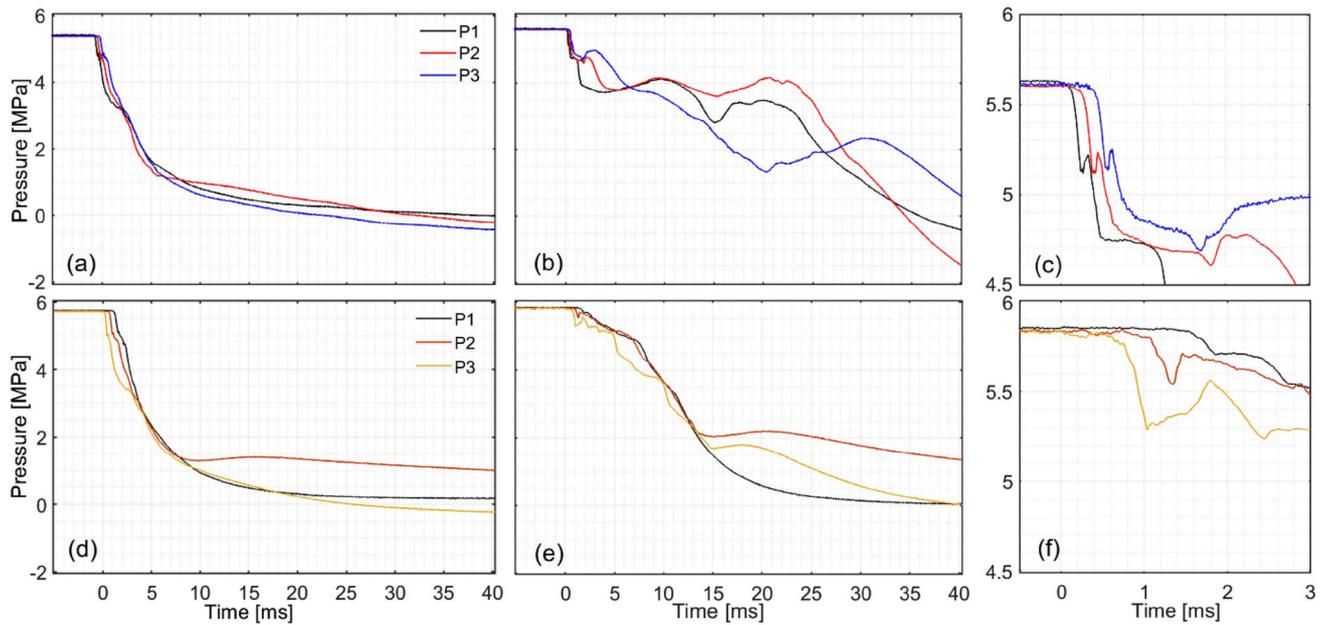


Fig. 7 Comparison of pressure histories during 40 ms of CO₂ depressurization in the rectangular duct's release from the top **a** and **b** and the bottom **d** and **e**. **c** and **f** are close-ups covering 3 ms

of **b** and **e**. The LVFs are 0% in **a** and **d**, 68.4% in **b**, and 66% in **e**. Graphs **a** and **b** from [13]

that the expansion and evaporation waves travel in and outside the container in three directions, including the jet flash evaporation at the bottom. But, they are restricted to the container wall during TR tests.

3.3 Shadowgraph images analysis

Fig. 8 shows a sequence of cropped images from shadowgraph video frames and corresponding pressure records during 4.5 ms of CO₂ liquid evaporation with LVF of 35%, while Fig 9 illustrates LVF of 58%. The time step between frames in both image sequences is 0.1 ms.

Images show the onset of the evaporation process at the surface, separating the liquid from vapor in the dark

region of shadowgraphs which increasingly expanded into the entire geometry. This dark zone was getting thicker due to liquid evaporation and two-phase mixture formation. The dark zone could have arisen from distortion and blockage of the light rays. Its emergence corresponds to density gradients, primarily because tiny bubbles make the fluid untransparent. The switch in the intensity of the grayscale pattern coincided with the changes in the pressure profiles. For example, in Fig. 9a, the pressure decreased abruptly between 372 and 372.5 ms and then peaked at about 373 ms. The darker area between 372 and 373 ms coincides with a pressure drop on P3 (installed at $h = 156$ mm). The darker area is assumed to be heterogeneous wall nucleation.

Fig. 8 Sequence of cropped images processed from shadowgraph videos and synchronized pressure records during liquid CO₂ release from the duct's bottom for LVF of 35%

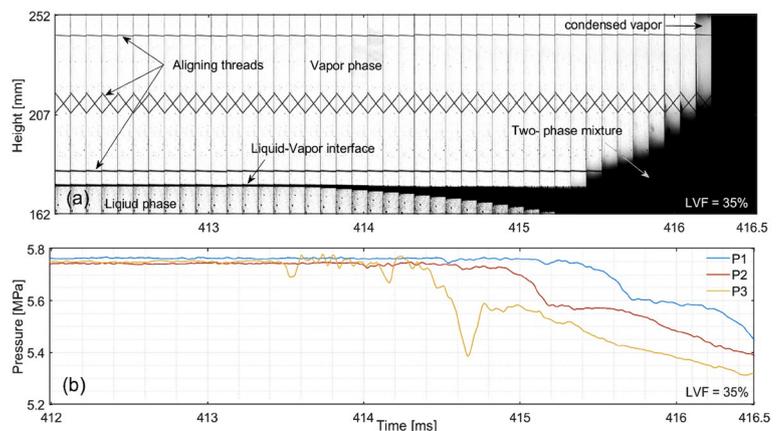


Fig. 9 Chronological series of shadowgraph images and corresponding pressure records during the release of liquified CO₂ from the bottom of a rectangular duct for LVF of 58%

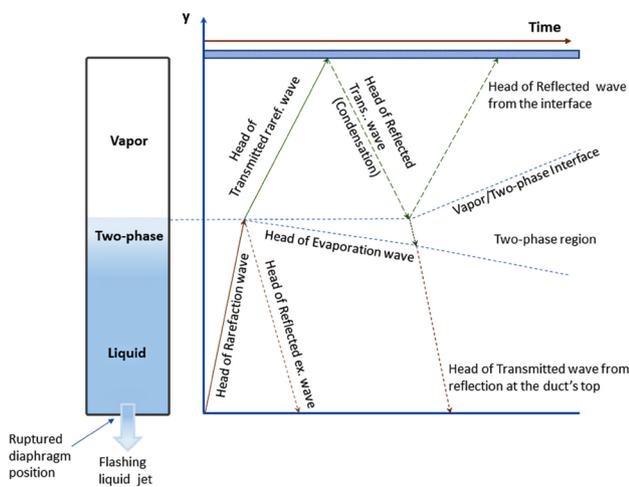
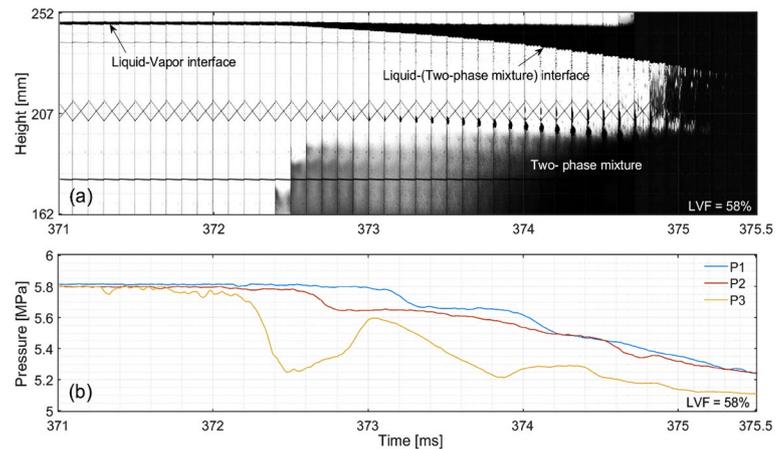


Fig. 10 Time-distance diagram showing the head of rarefaction waves, the evaporation wave, and the two-phase interface inside the duct. (The velocities of the waves are not drawn to scale)

Then it toned down and further intensified as the pressure declined.

The wave configuration during the phase transition is quite complex due to wave interactions between the primary, transmitted through the liquid/vapor interface, and reflected waves. Figure 10 is a time-distance diagram showing the head of rarefaction waves, the evaporation wave, and the two-phase interface inside the duct.

As the diaphragm ruptured, an expansion wave propagated upward inside the duct. Instantaneously, a shock wave propagated downwards into the atmosphere, followed by an expanded multiphase jet (not shown in the figure). The rarefaction wave propagated upwards through the liquid and vapor headspace. While it transmitted through the liquid/vapor interface into the vapor phase, it was also reflected back into the liquid. The expanded liquid became superheated for a while before the evaporation

started. When the rarefaction transmitted wave reached the duct's top, it was reflected into expanded saturated vapor. Then part of it was reflected at the two-phase/vapor interface while transmitted into the two-phase mixture.

During vapor expansion, it partially condenses due to the head of the transmitted rarefaction wave propagation. The partial vapor condensation occurs at the upper duct part as the expansion waves reach the duct ceiling and reflect into the vapor phase. As shown in Fig. 4, the shadowgraph imaging area does not include the upper duct's height. However, in Fig. 8a, a part of the condensed vapor is observable in the upper right corner. To capture more details, Fig. 11 demonstrates (a) shadowgraph images for LVF of 35% presented in Fig. 8a and an enlarged image (b) covering the frames during 0.1 ms indicated in a red box in picture (a). It depicts the process occurring in the vapor phase region during the break up of the vapor/liquid interface. Calculations based on the Span-Wagner EOS [16] demonstrated that the expanded fluid had a vapor quality of 0.93 after the saturated vapor isentropic expansion. This result verifies the abovementioned observation about partial vapor condensation in Fig. 8a.

The pressure records were drawn on the duct height-time scale to show the wave trajectories. The points on the pressure curves of observable inclines signify waves' paths that follow the defined time points at the fixed pressure sensors' positions [14]. Figure 12 illustrates pressure histories between 5.8 and 5.2 MPa drawn on the duct height scale during 4.5 ms of liquified CO₂ depressurization for LVFs of 35% in (a) and 58% in (b). The dashed lines indicate the head of expansion waves' trajectories, where the first line corresponds to the pressure drop due to the diaphragm rupturing. The reflected waves are not shown in this figure, but a detailed explanation of reflected and transmitted waves is given in Fig. 10. The following lines relate to the expansion waves arising from pressure decline and the subsequent occurrence of

Fig. 11 **a** Sequence of shadowgraph images during liquid CO₂ release from the duct's bottom for LVF of 35%. **b** Close-up including the frames shown in a red box in the picture **a**

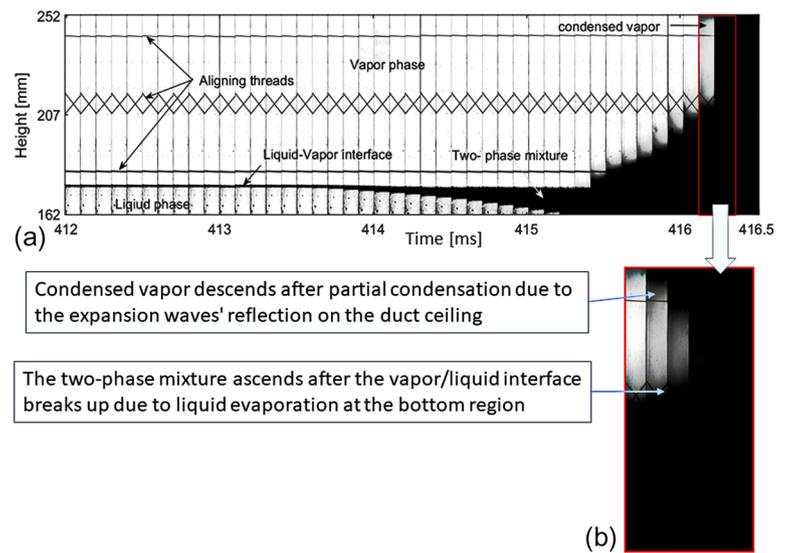
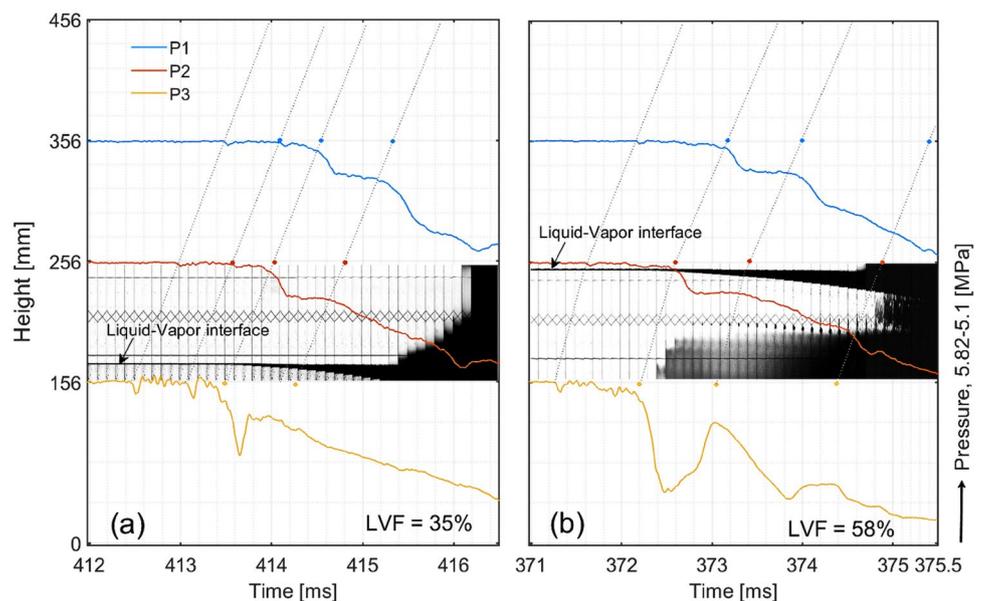


Fig. 12 Height-time diagram demonstrating pressure transducer readings on vessel height-axis during 4.5 ms of liquified CO₂ release from the duct's bottom side. For LVFs of 35% in **a** and 58% in **b**. The shadowgraph images were displayed at the corresponding height position



heterogeneous nucleation on the duct's wall. That can be seen as the emergence of the grayscale pattern at about 372.4 ms after the second dashed line in Fig. 12b. Then the sequent expansion wave lines followed the decline in fluctuated pressure curves and the bubble's development (see Fig. 10). Chiefly, they were tracked by the pattern of bubbles' collisions, coalescence, and movement upward until joining to the diffusing two-phase mixture as the evaporation wavefront propagated downward (at about 374.8 ms in Fig. 12b).

The graphs in Fig. 12 include the cropped shadowgraph images for the stated LVFs. Point 0 on the height axis refers to the diaphragm position (see Fig. 4). The rarefaction wave velocities were analyzed graphically

based on the identified time points where the first pressure dropped after rupturing. The method details are given in [14]. The uncertainty in velocities calculation resulted from the measurement errors of time turning points where the pressure declined. The accuracy of measurement errors depends on how sharp the pressure lines change their direction downwards. Subsequently, the uncertainties in velocity calculations were estimated as an average of measurements with standard error. The mean calculated velocity for the rarefaction wave after the first sudden pressure drop for the LVF of 35% was 200 ± 2 m/s, while for 58% was 266 ± 2 m/s. Table 1 summarizes the initial (pre-rupture) conditions and the calculated rarefaction velocities for

Table 1 Initial conditions and calculated rarefaction wave velocities from two experimental series

Description	Unit	Test series 1				Test series 2	
Pre-rupture pressure	MPa	5.86	5.86	5.85	5.94	5.77	5.81
Pre-rupture temperature	°C	22.3	22.2	22.2	22.2	19.9	20.4
Liquid volume fraction (LVF)	%	29.0	53.0	66.0	97.0	35.0	58.0
*Rarefaction wave velocity (zone P1-P2)	m/s	200.0	204.0	267.0	285	–	–
*Rarefaction wave velocity (zone P2-P3)	m/s	200.0	229.0	279.0	299	–	–
**Rarefaction wave velocity (shadowgraph)	m/s	–	–	–	–	200.0	266.0

*The calculation errors were estimated ± 8 m/s, and for ** values were ± 2 m/s

the first experimental series (four different LVFs are presented) and the second series with shadowgraph imaging, including two LVFs.

The liquid, and the vapor, were at equilibrium before the diaphragm ruptured. In Fig. 7, it can be observed that the interface was nearly equable. When the diaphragm ruptured, interfacial perturbations emerged due to the pressure drop and the rarefaction wave propagation penetrating the interface. In the first phase after the diaphragm rupture, instabilities in some spots at the interface were a pattern of tiny spikes that developed over time. This phenomenon is described by Hill [9], where a colder liquid layer was temporarily shaped at the surface and became denser than the liquid underneath. Then it was displaced by a warmer liquid while the liquid's level decreased due to the high mass and heat transfer rate at the interface. The shadowgraph images in Figs. 8 and 9 show that the expanded vapor accelerated into the denser liquid, creating a bubbly mixture that propagated downwards. The thickness of the two-phase interface layer was also increased due to the bubbles arising from heterogeneous nucleation on the duct's wall. It is unclear from the planar shadowgraph images whether the two-phase layer expansion is due to the surface, bulk, or boundary layer effect. However, the images showed that the liquid/vapor interface developed into a two-phase mixture and remained nearly constant. While a second liquid/two-phase mixture interface was formed, developing downward in the liquid. This is opposed to TR experiments wherein the initial liquid/vapor contact surface (and downstream two-phase mixture) propagated upwards immediately after the diaphragm rupture.

The shadowgraph images of the BR experiments showed further development by interface breaking up and propagating rapidly upwards. As the expansion wave propagated upwards through the vapor and reflected from the top, a condensation wave was observed to propagate behind. This trend can be seen

after 416.2 ms in Fig. 8a. Afterward, the two-phase fluid increased until it occupied the entire duct's volume.

4 Conclusions

Small-scale experiments were performed in a rectangular duct to understand phase transition during the release of liquified CO₂ from the bottom. The study sought to evaluate the expansion and evaporation wave behavior during phase transition and its contradiction with top releases. It is highly relevant to a BLEVE scenario considering accidental vessel rupture. Comparing the results from the current bottom release (BR) experiments with the previous top release (TR) results [13] reveals significant differences. The shadowgraph images from BR tests showed that the initial liquid/vapor contact surface remained flattened, almost horizontally, for a relatively long period before breaking up, then developing into a two-phase front trailing the expansion wave. In the TR tests, the liquid/vapor contact surface is immediately sucked out by the expansion wave.

The degree of superheating (DOS) in the BR tests was lower than in TR. For example, the DOS decreased by 34% for LVF = 66.0% (BR) compared to 68.4% (TR)). The pressure drop was 1.2–1.8 times faster during BR than TR tests, implying faster evaporation of the liquid. These results show that the evaporation rate depends on whether the rupture area is below or above the liquid level. This will likely affect the blast strength and fragment formation in accidental events involving ruptures of vessels containing liquid CO₂. The experimental results could also be used in model development for better risk assessment.

Finally, this study is restricted to the evaporation mechanism inside a duct during CO₂ release from the bottom. Further research studying the evaporation of the bottom outflowing flashing liquid jet and its effect on the blast wave intensity would give more insight into CO₂ tank explosion during release below the liquid level.

Author contributions All authors contributed to the study's conception and design. Material preparation, data collection, and analysis were performed by [OMI]. The first draft of the manuscript was written by [OMI], and all authors commented on previous versions of the manuscript. Investigation resources were facilitated by [PMH], [AVG], [DB], and [KV]. The research was administered by [KV]. All authors read and approved the final manuscript.

Funding This research was funded by our institution: The University of South-Eastern Norway, USN.

Data availability The dataset that supports research findings is published in Mendeley Data, and the link is given in (M Ibrahim 2023).

Declarations

Conflict of interest The authors declare there are no conflicts of interest relevant to the content of this article.

Ethical approval This declaration is "not applicable" Human participants and animals are not involved in this research.

Open Access This article is licensed under a Creative Commons Attribution 4.0 International License, which permits use, sharing, adaptation, distribution and reproduction in any medium or format, as long as you give appropriate credit to the original author(s) and the source, provide a link to the Creative Commons licence, and indicate if changes were made. The images or other third party material in this article are included in the article's Creative Commons licence, unless indicated otherwise in a credit line to the material. If material is not included in the article's Creative Commons licence and your intended use is not permitted by statutory regulation or exceeds the permitted use, you will need to obtain permission directly from the copyright holder. To view a copy of this licence, visit <http://creativecommons.org/licenses/by/4.0/>.

References

1. CCPS (2010) Guidelines for vapor cloud explosion, pressure vessel burst, BLEVE, and flash fire hazards, 2nd edn. Center for Chemical Process Safety, AIChE-Wiley, New York, pp 311–360
2. Zhang Y, Schork J, Ludwig K (2013) Revisiting the conditions for a CO₂ tank explosion. Proceedings of the 9th Global Congress on Process Safety, AIChE, San Antonio, Texas, pp. 109–120.
3. Angelo E, Simões-Moreira JR, Barrios DB (2005) Theory and occurrence of evaporation waves. Proceedings of the 18th International Congress of Mechanical Engineering, Ouro Preto, Minas Gerais, Brazil. <https://www.abcm.org.br/anais/abcm/2005/PDF/COBEM2005-0475.pdf>. Accessed October 2022
4. Reinke P (1997) Surface boiling of superheated liquid. Dissertation, Mechanical Engineering ETH, Zurich, Switzerland. http://inis.iaea.org/search/search.aspx?orig_q=RN:28030620. Accessed October 2022.
5. Vieira MM, Simões-Moreira JR (2007) Low-pressure flashing mechanisms in iso-octan liquid jets. *J Fluid Mech* 572:121–144. <https://doi.org/10.1017/S0022112006003430>
6. Hansen PM, Gaathaug AV, Bjerketvedt D, Vaagsaether K (2019) Rapid depressurization and phase transition of CO₂ in vertical ducts – small-scale experiments and Rankine-Hugoniot analyses. *J Hazard Mater* 365:16–25. <https://doi.org/10.1016/j.jhazmat.2018.10.092>
7. Dewangan KK, Das PK (2020) Experimental analysis of flashing front propagation in superheated water: effects of degree of superheat, tube inclination, and secondary nucleation. *Phys Fluids* 32:7. <https://doi.org/10.1063/5.0006840>
8. Simões-Moreira JR (1994) Adiabatic evaporation waves. Dissertation, Rensselaer Polytechnic Institute, Troy, N.Y. <https://books.google.no/books?id=mJigtgAACAAJ>
9. Hill LG (1991) An experimental study of evaporation waves in a superheated liquid. Dissertation, California Institute of Technology, Pasadena, California. <https://resolver.caltech.edu/CaltechETD:etd-10242005-103224>. Accessed November 2022
10. Venart JES, Rutledge GA, Sumathipala K, Sollows K (1993) To BLEVE or not to BLEVE: anatomy of a boiling liquid expanding vapor explosion. *Proc Saf Prog* 12:67–70. <https://doi.org/10.1002/prs.680120202>
11. Tosse S, Vaagsaether K, Bjerketvedt D (2014) An experimental investigation of rapid boiling of CO₂. *Shock Waves* 25:277–282. <https://doi.org/10.1007/s00193-014-0523-6>
12. Shang Q, Tian Z, Wang S, Hua M, Pan X, Shi S, Jiang J (2022) Experimental research on the two-phase explosive boiling mechanism of superheated liquid under different leakage conditions. *Appl Thermal Eng* 216:119080. <https://doi.org/10.1016/j.applthermaleng.2022.119080>
13. Hansen PM (2018) Experimental and theoretical studies of rapid phase transitions in carbon dioxide Dissertation, University of South-Eastern Norway <https://openarchive.usn.no/usnxmlui/handle/11250/2587457?show=full>. Accessed October 2022
14. Ibrahim OM, Hansen PM, Bjerketvedt D, Vågsæther K (2021) Evaporation characteristics during decompression of liquified CO₂ from a conical-shaped vessel. *Results Eng* 12:1–8. <https://doi.org/10.1016/j.rineng.2021.100304>
15. Span R, Wagner W (1996) A new equation of state for carbon dioxide covering the fluid region from the triple-point temperature to 1100 K at pressures up to 800 MPa. *J Phys Chem Ref Data* 25:1509–1596. <https://doi.org/10.1063/1.555991>
16. Mjaavatten A (2021) Thermodynamic models and tools for H₂O, H₂, CO₂, and Air. GitHub <https://github.com/are-mj/thermodynamicsGitHub>. Accessed November 2022
17. M Ibrahim O (2023) Release of liquid CO₂ from the bottom of a duct. Mendeley Data, V1, <https://data.mendeley.com/datasets/yzsp69gptd/1>

Publisher's Note Springer Nature remains neutral with regard to jurisdictional claims in published maps and institutional affiliations.